

# Influence of $\text{LiNO}_3$ on the Lithium Metal Deposition Behavior in Carbonate-Based Liquid Electrolytes and on the Electrochemical Performance in Zero-Excess Lithium Metal Batteries

Silvan Stuckenberg, Marlena Maria Bela, Christian-Timo Lechtenfeld, Maximilian Mense, Verena Küpers, Tjark Thorben Klaus Ingber, Martin Winter,\* and Marian Cristian Stan\*

Continuous lithium (Li) depletion shadows the increase in energy density and safety properties promised by zero-excess lithium metal batteries (ZELMBs). Guiding the Li deposits toward more homogeneous and denser lithium morphology results in improved electrochemical performance. Herein, a lithium nitrate ( $\text{LiNO}_3$ ) enriched separator that improves the morphology of the Li deposits and facilitates the formation of an inorganic-rich solid–electrolyte interphase (SEI) resulting in an extended cycle life in  $\text{Li}||\text{Li}$ -cells as well as an increase of the Coulombic efficiency in  $\text{Cu}||\text{Li}$ -cells is reported. Using a  $\text{LiNi}_{0.6}\text{Co}_{0.2}\text{Mn}_{0.2}\text{O}_2$  positive electrode in  $\text{NCM622}||\text{Cu}$ -cells, a carbonate-based electrolyte, and a  $\text{LiNO}_3$  enriched separator, an extension of the cycle life by more than 50 cycles with a moderate capacity fading compared to the unmodified separator is obtained. The relative constant level of  $\text{LiNO}_3$  in the electrolyte, maintained by the  $\text{LiNO}_3$  enriched separator throughout the cycling process stems at the origin of the improved performance. Ion chromatography measurements carried out at different cycles support the proposed mechanism of a slow and constant release of  $\text{LiNO}_3$  from the separator. The results indicate that the strategy of using a  $\text{LiNO}_3$  enriched separator instead of  $\text{LiNO}_3$  as a sacrificial electrolyte additive can improve the performance of ZELMBs further by maintaining a compact and thus stable SEI layer on Li deposits.


## 1. Introduction

Despite the continuous increase of their applicability in our modern life, lithium-ion batteries (LIBs) are reaching their theoretical limits in terms of capacity and energy density.<sup>[1]</sup> Lithium–metal batteries (LMBs) were longtime valued for their increased energy density and specific energy,<sup>[2]</sup> however, a series of challenges limit their widespread commercialization.<sup>[3]</sup> Compared to graphite anodes with a Li storage capacity of  $372 \text{ mAh g}^{-1}$ , lithium-metal anodes (LMAs) show much higher specific capacities ( $3860 \text{ mAh g}^{-1}$ ) with the lowest potential of all metallic anode materials ( $-3.04 \text{ V}$  vs standard hydrogen electrode, (SHE)). However, LMAs suffer from several challenges such as inhomogeneous Li electrodeposition, respectively high surface area lithium (HSAL) growth and limited Coulombic efficiency (CE) caused by the formation of electrochemically inactive cycled Li metal (“dead” Li) and parasitic side reactions due to the high reactivity of Li metal with nearly all dipolar aprotic organic solvents.<sup>[4–7]</sup>

Besides these general problems, an excess of Li metal to counterbalance Li losses in LMAs leads to further drawbacks. For example, an excess of 200% Li metal decreases the theoretical volumetric capacity from  $2060$  to  $687 \text{ mAh cm}^{-3}$ , a value that is even below that of commonly used graphite anodes (i.e.,  $719 \text{ mAh cm}^{-3}$  for  $\text{LiC}_6$ ).<sup>[8,9]</sup> Furthermore, higher amounts of Li metal in these cells would also increase the safety concerns due to the high reactivity and high energy content of Li metal in general.<sup>[10,11]</sup> Therefore, the amount of Li metal should be kept as low as possible, as is in the case of ultrathin Li metal electrodes ( $<30 \text{ }\mu\text{m}$ ),<sup>[12,13]</sup> or using negative electrodes without any Li metal excess, respectively, no Li metal in the discharged state.<sup>[8]</sup> In such concepts, known as anode-free or zero-excess lithium metal batteries (ZELMBs), initially, all the electrochemically active Li ions are stored within the layered structure of the cathode active material (CAM). This can simplify the cell manufacturing process compared to present

S. Stuckenberg, M. M. Bela, C.-T. Lechtenfeld, M. Mense, V. Küpers, T. T. K. Ingber, M. Winter, M. C. Stan  
MEET Battery Research Center  
University of Münster  
Corrensstraße 46, 48149 Münster, Germany  
E-mail: m.winter@fz-juelich.de; marian.stan@uni-muenster.de

M. Winter  
Helmholtz-Institute Münster (HI MS)  
IEK-12  
Forschungszentrum Jülich GmbH  
Corrensstraße 46, 48149 Münster, Germany

 The ORCID identification number(s) for the author(s) of this article can be found under <https://doi.org/10.1002/smll.202305203>

© 2023 The Authors. Small published by Wiley-VCH GmbH. This is an open access article under the terms of the Creative Commons Attribution License, which permits use, distribution and reproduction in any medium, provided the original work is properly cited.

DOI: 10.1002/smll.202305203

LIB technology.<sup>[14]</sup> During the initial discharge process, Li ions are removed from the CAM, transported through the electrolyte to the anode, and electrodeposited as Li metal on the bare current collector (e.g., Cu). Such a current collector material usually has a higher density than Li, thus the specific energy compared to Li as a substrate for deposition is negatively affected. In ZELMBs, the lack of an excess of Li metal at the negative electrode requires a high CE for the electrochemical cycling processes. It has been shown that side reactions at both electrodes affect the CE, with the electrolyte decomposition and Li loss due to the formation of dead Li being the major undesired processes occurring at the negative electrode.<sup>[15]</sup> Hence, high capacity retention with high CE and a dense, low surface area Li deposition morphology are among the main goals for ZELMBs.<sup>[16,17]</sup>

Intrinsic formation of inhomogeneous and porous Li deposits resulting in severe surface area variations is another factor enhancing further side reactions.<sup>[17,18]</sup> To overcome such challenges and to preserve the advantages promised by ZELMBs, many strategies are focusing on the identification of suitable substrate architectures,<sup>[19–22]</sup> or using surface coatings with lithiophilic properties.<sup>[23–26]</sup> In addition, optimization of the testing procedure, temperature, and cell fabrication can improve the active Li inventory retention.<sup>[8,15,27]</sup> Moreover, much attention is directed toward the electrolyte formulation, as the reactivity of Li metal with liquid electrolytes leads to the formation of a solid–electrolyte interphase (SEI) layer. This reaction can be used to engineer stable SEI films that protect the Li deposits and thus reduce the side reactions. Among many strategies, the use of salt blends was shown to improve the cycle life of ZELMBs,<sup>[27–30]</sup> while the use of electrolyte additives also improved the quality of the SEI layer.<sup>[31–33]</sup>

Lithium nitrate ( $\text{LiNO}_3$ ) is a widely used additive in ether-based sulfur || Li and oxygen || Li batteries<sup>[18,34–38]</sup> as well as in ZELMB systems<sup>[39]</sup> due to its ability to form a nitrogen-rich SEI which protects the Li anode from further side reactions. However, since  $\text{LiNO}_3$  is poorly soluble in carbonate-based electrolytes, various methods to increase its content were considered including the use of a pre-impregnated separator membrane,<sup>[40]</sup> solid cathode additives,<sup>[41,42]</sup> and the use of pyridine to increase the  $\text{LiNO}_3$  solubility in the carbonate-based electrolyte.<sup>[43]</sup> Regardless of the approach, the presence of the  $\text{LiNO}_3$  decomposition products on the LMA surface results in improved performance.

Herein, we report about the beneficial role of  $\text{LiNO}_3$  on the Li metal electrodeposition and dissolution in ZELMBs using carbonate-based liquid organic electrolytes. Using a  $\text{LiNO}_3$  enriched separator and a carbonate-based electrolyte (1 M  $\text{LiPF}_6$  in EC/EMC (3:7 wt%)), a higher CE was shown in cells with excess Li metal (Cu || Li, with a 12 mm diameter Li metal anode and a capacity of  $30.9 \text{ mAh cm}^{-2}$ ) compared to the reference setup. Besides, the morphology of the lithium deposits was also observed to be positively affected by the presence of  $\text{LiNO}_3$ . Moreover, without an excess of Li, i.e., using Cu as a negative electrode and NCM622 as CAM, the  $\text{LiNO}_3$ -modified separators result in a more stable cycling performance and reduced capacity fading for more than 50 cycles. The high Li electrodeposition and dissolution efficiency in such ZELMB cells is enabled by the presence of  $\text{LiNO}_3$  decomposition products at the surface of freshly deposited Li metal. It is also shown that the modification of the separator with  $\text{LiNO}_3$  results in a continuous and slow release of

the additive into the electrolyte, supporting a high performance of the beneficial electrochemical reaction mechanism of  $\text{LiNO}_3$  over many cycles. By combining the presented approach with other engineered materials, an important technological step in the pathway of both ZELMBs and conventional LMBs realization can be taken.

## 2. Results and Discussion

The effect of  $\text{LiNO}_3$  as an electrolyte additive on the performance of LMBs has been intensively studied for various electrolyte blends, in particular for its role in creating a protective film on the LMA surface.<sup>[43,47–50]</sup> Although through its decomposition and the subsequent formation of a beneficial protective layer on the Li metal surface consisting of both inorganic ( $\text{Li}_2\text{O}$ ,  $\text{LiN}_x\text{O}_y$ , and  $\text{Li}_3\text{N}$ ) as well as organic (ROLi,  $\text{ROCO}_2\text{Li}$ ) species,<sup>[51]</sup>  $\text{LiNO}_3$  is considered to be a “sacrificial electrolyte additive” since it is reacting with deposited Li metal in each cycle. In other words, since  $\text{LiNO}_3$  is continuously consumed, the beneficial effect is maintained as long as the salt is present in the electrolyte solution, and upon its depletion, the electrochemical performance will deteriorate. In this work, a modified separator stack with  $\text{LiNO}_3$  can be used to provide further understanding on the effect of the  $\text{LiNO}_3$  on the electrochemical performance of ZELMBs in carbonate-based electrolytes and—through slow, but continuous release of the additive over time—to exceed the beneficial influence over a large number of cycles. SEM images of the separators before and after the modification are presented in **Figure 1**.

Compared to the pristine separators (Figure 1a,b), the SEM images confirm the presence of  $\text{LiNO}_3$  particles both on top of the microporous Cg 2500 membrane as well as within the nonwoven structure of the FS 2190 separator after the addition of the  $\text{LiNO}_3$  solution to the separator stack followed by the vacuum removal of the solvent (Figure 1c,d; Figure S1, Supporting Information). No additional changes in the separator morphology can be observed. SEM with elemental analysis (EDX) was used to prove the composition of the particles as  $\text{LiNO}_3$  (Figure S2, Supporting Information) while the XRD investigations indicated that there are no structural changes between the pristine  $\text{LiNO}_3$  particles and the particles present in the modified separator (Figure S3, Supporting Information). The presence of oxygen and nitrogen in the area of the particles verifies the successful  $\text{LiNO}_3$  modification of the separator stack. Based on the weight of the dried separator stacks, the total amount of  $\text{LiNO}_3$  in the treated separators was found to be  $\approx 1.3 \text{ mg cm}^{-2}$ .

The effect of modification with  $\text{LiNO}_3$  on the constant current performance was studied by assembling the modified separator stack into electrochemical Cu || Li cells where CE, overvoltage of the Li electrodeposition/dissolution process, and cycle life were assessed. An overview of the performance of Cu || Li cells with the  $\text{LiNO}_3$  modified separators and the carbonate-based electrolyte is provided in **Figure 2**.

The presence of  $\text{LiNO}_3$  in the modified separator results in a substantial extension of Cu || Li cell's cycle life by more than 400 h (Figure 2a) compared to a cell with an unmodified separator. In these experiments, it is also noticeable that the upper voltage limitation of 1.5 V is continuously reached for both cells. Therefore, part of the electrodeposited Li is also consumed by irreversible reactions involving electrolyte decomposition

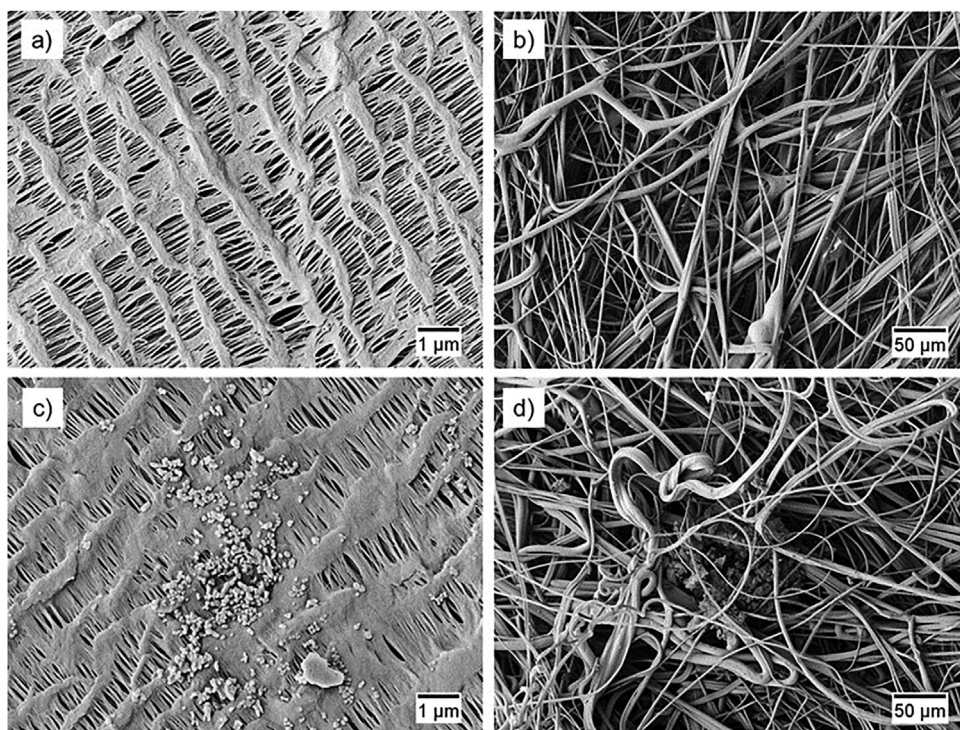


**Figure 1.** SEM images of pristine a) Cg 2500 and b) FS 2190 separators and after the addition and subsequent drying of 120  $\mu\text{L}$   $\text{LiNO}_3$  solution, showing the deposited solid  $\text{LiNO}_3$  c) Cg 2500 and d) FS 2190 separators. The SEM images were taken at 10 000 $\times$  magnification for Cg 2500 and at 250 $\times$  magnification for FS 2190. All samples were gold-sputtered for 20 s to avoid surface charging during SEM visualization.

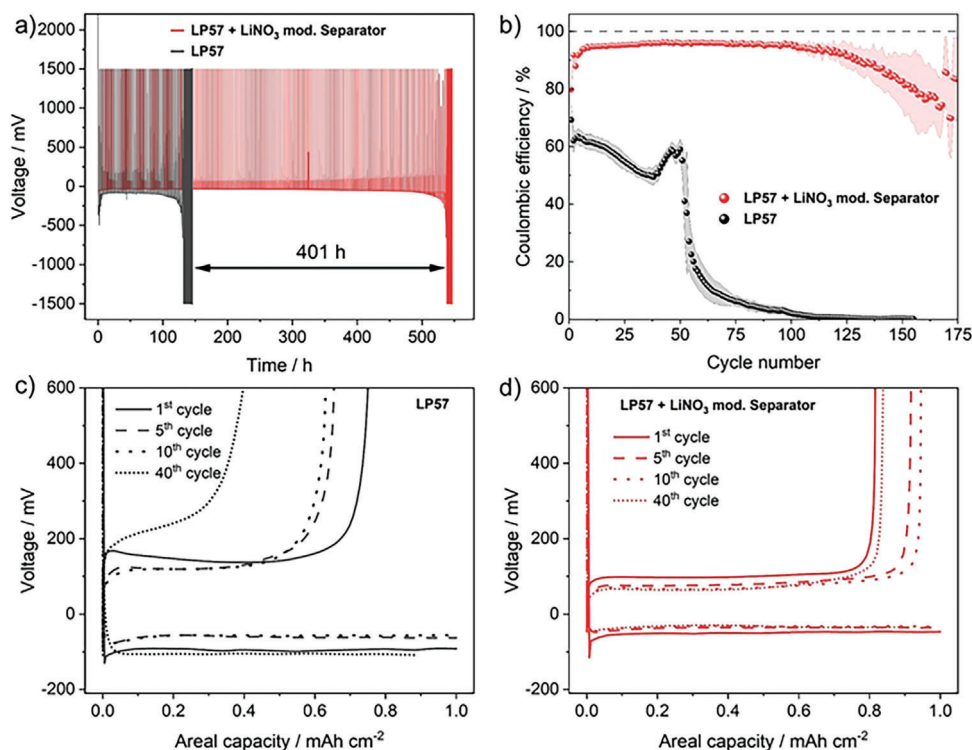


**Figure 2.** a) Cell voltages and b) corresponding CE of Cu || Li cells with and without  $\text{LiNO}_3$  modification of the separator stack cycled using a current density of 0.5  $\text{mA cm}^{-2}$  for Li electrodeposition and 1.25  $\text{mA cm}^{-2}$  for Li electrodisolution to a total capacity transferred per step of 1  $\text{mAh cm}^{-2}$ . Voltage profiles for selected cycles c) without and d) with  $\text{LiNO}_3$  modified separator stack.



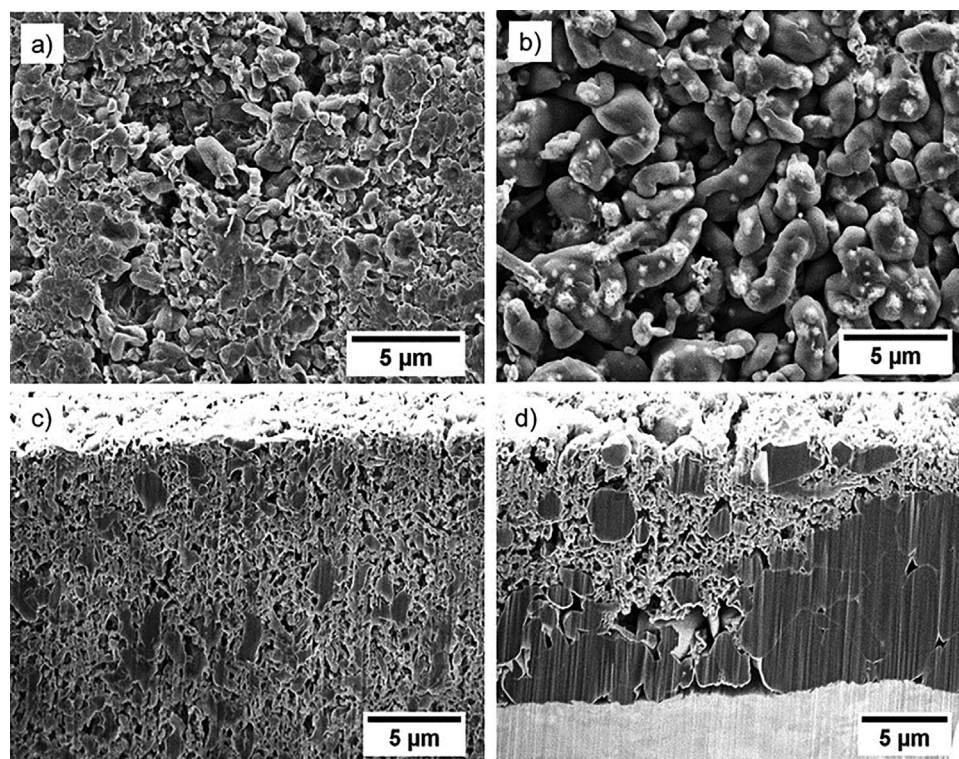


**Figure 3.** SEM images of the top view of Li deposits after the first electrodeposition (a,b) and cross-section morphology of the Li deposits after 20 cycles and a subsequent electrodeposition step (c,d) from Cu || Li cells. The cells were cycled with a current density of  $0.5 \text{ mA cm}^{-2}$  for Li electrodeposition and  $1.25 \text{ mA cm}^{-2}$  for Li dissolution using (a,c) LP57 electrolyte with unmodified separator and (b,d) LP57 electrolyte with  $\text{LiNO}_3$  modified separator.

(SEI formation) and formation of dead Li leading to less Li that can be electrochemically dissolved as compared to the amount of Li that is electrodeposited in each cycle. A better overview of the amount of the irreversible reactions is provided by the CE of Cu || Li cells (Figure 2b), defined as the ratio of the amount of Li dissolved from the Cu current collector to that of the Li deposited on the Cu current collector during each electrodeposition/deposition cycle. The cells with  $\text{LiNO}_3$ -modified separators show a higher CE of 79.7% for the first electrodeposition/dissolution cycle than the cells with pristine separator of 69.0%. On prolonged cycling, the Li electrodeposition/dissolution process of the cell with the  $\text{LiNO}_3$  modified separator occurred with an efficiency of 95.0% for 120 cycles. In contrast, the cycling behavior of Cu || Li cells with unmodified separators (Figure 2a) is deteriorating already after 130 h, meanwhile a CE of 56.9% is obtained before the Li electrodeposition/dissolution process fails after 50 cycles (Figure 2b). The evolution of the Li electrodeposition/dissolution overvoltages during the 1st, 5th, 10th, and 40th cycles are presented in Figure 2c,d. The cells with pristine separators show increasing overvoltages from the 1st to the 40th cycle. Lower overvoltages with no significant change are observed for Cu || Li cells with  $\text{LiNO}_3$  modified separator. These results underline the beneficial effect of the presence of  $\text{LiNO}_3$  in the electrolyte solution leading most likely to the formation of an efficient SEI layer. Similarly, an improved cycle life with lower overvoltages is also observed when  $\text{LiNO}_3$  modified separators are used in Li || Li-symmetrical cells with excess of Li at the LMA (Figure S4, Supporting Information).

Postmortem analysis of the Cu electrodes after the 1st and the 20th cycles of Li electrodeposition/dissolution was carried out by recording the SEM and cryo-FIB-SEM images of the electrodes recovered from Cu || Li cells (Figure 3).

The initial Li electrodeposition of the cell with the unmodified separator shows an uneven and heterogeneous morphology (Figure 3a). In this case, large amounts of Li and electrolyte are consumed during the formation of an unstable and thick SEI, as was previously shown also by the poor CE during the 1st electrodeposition step. On the contrary, the  $\text{LiNO}_3$ -modified separator enables the formation of smooth and non-dendritic Li deposits (Figure 3b). It is also recognized that a decreased surface area of the Li deposits or the formation of low surface area lithium (LSAL) and a smooth Li deposition lead to better safety, higher CE, and longer cycle life, and is influenced strongly by the composition of the electrolyte.<sup>[52]</sup> Cryo-FIB-SEM was used to gain further insight into the bulk morphology of such Li deposit (Figure 3c,d). After 20 cycles of Li electrodeposition/dissolution and one subsequent electrodeposition step on the Cu current collector, the Li morphology with an unmodified separator shows mossy and loosely packed Li deposits with HSAL, while the presence of  $\text{LiNO}_3$  in the separator results in dense Li deposits. These results further support the hypothesis that the nature of the SEI and the Li morphology are crucial for a high CE of the Li electrodeposition/dissolution process, with the CE being a key parameter characterizing the performance of every ZELMB.

For sulfur || Li cells, it is generally acknowledged that  $\text{LiNO}_3$  in ether-based electrolytes is reduced on the surface of the

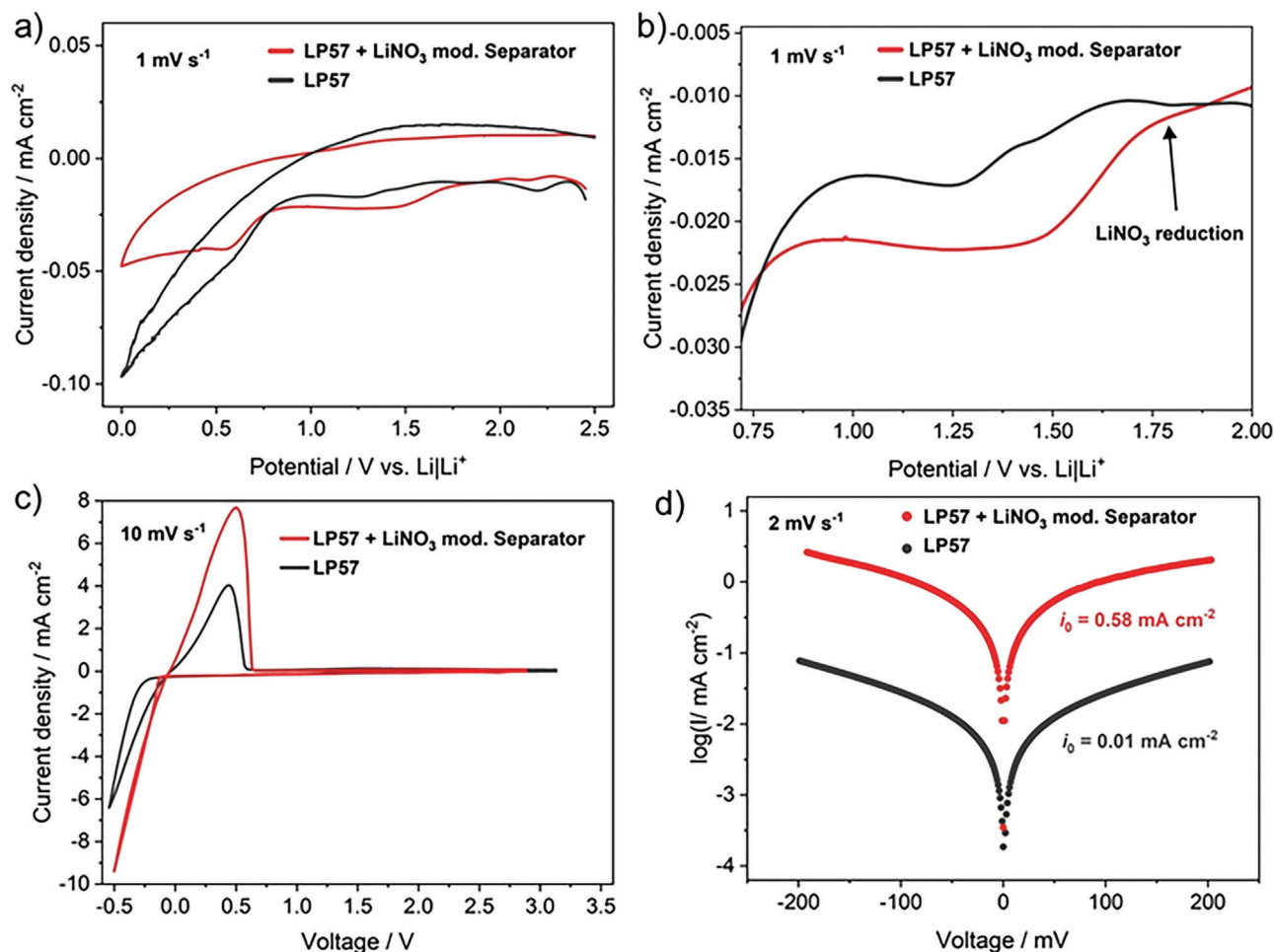


**Figure 4.** a) Cyclic voltammograms of 3-electrode Cu || Li cells with Li reference electrode without and with LiNO<sub>3</sub> modification of the separator in a potential range of 0 V ≤ E ≤ 2.5 V versus Li|Li<sup>+</sup> with a sweep rate of 1 mV s<sup>−1</sup>. b) Magnification of the potential range where LiNO<sub>3</sub> is reduced. c) Cyclic voltammogram of 2-electrode Cu || Li cells without and with LiNO<sub>3</sub> modification of the separator in a voltage range between OCV ≤ U ≤ −0.5 V with a sweep rate of 10 mV s<sup>−1</sup>. d) Tafel plots obtained from LSV measurements in symmetric Li || Li cells and the corresponding exchange current densities calculated from the voltage range of 0.08 ≤ U ≤ 0.20 V. All measurements were carried out at 20 °C.

sulfur cathode starting already at 1.6 V versus Li|Li<sup>+</sup>, leading passivation films on the sulfur and on the LMA.<sup>[53]</sup> To investigate the electrochemical decomposition of LiNO<sub>3</sub> in carbonate-based electrolytes, cyclic voltammetry and LSV measurements were carried out (Figure 4). Cyclic voltammetry of three-electrode Cu || Li cells with Li metal as the reference electrode was carried out in the potential range of 2.5–0 V versus Li|Li<sup>+</sup> in order to investigate the electrochemical stability of LiNO<sub>3</sub>. In this potential range, LiNO<sub>3</sub> can be decomposed reductively without any electrodeposition of Li metal to occur in parallel (Figure 4a,b). In the CV of the Cu || Li cell with a LiNO<sub>3</sub>-modified separator, a reduction process is observed starting at ≈1.8 V versus Li|Li<sup>+</sup> with its maximum current reached at 1.5 V versus Li|Li<sup>+</sup>. In contrast, the cell without LiNO<sub>3</sub> shows only a small reduction peak around 1.25 V versus Li|Li<sup>+</sup> that is possibly due to the reduction of the carbonate-based solvents, SEI formation, and side reactions with the Cu surface components. The reduction peak at around 2.25 V versus Li|Li<sup>+</sup> contributes to the reduction of CuO present at the surface of the copper current collector.<sup>[54]</sup> Constant current experiments of Cu || Li

cells, with and without LiNO<sub>3</sub> separator, at a current density of 0.05 mA cm<sup>−2</sup> pointed out the reductive processes during the first electrodeposition on a copper current collector. Both cells show a similar voltage drop within the first 15 s, however, the cells with LiNO<sub>3</sub> modified separator show a small plateau around 1.8 V assigned to LiNO<sub>3</sub> reduction (Figure S5, Supporting Information). This result is in agreement with the CV measurements presented in Figure 4a,b.

It is also observed that the intensity of the reductive currents below 0.5 V versus Li|Li<sup>+</sup>, is low and independent of LiNO<sub>3</sub> presence, thus no electrodeposition of Li metal occurs in this potential range.<sup>[55]</sup> When increasing the potential range to −0.5 V versus Li|Li<sup>+</sup>, a sharper current peak of the Li electrodeposition/dissolution reaction is seen for the cell with the LiNO<sub>3</sub>-modified separator as compared to the unmodified cell (Figure 4c). The amount of charge during the cathodic scan (reduction, i.e., Li electrodeposition) without and with LiNO<sub>3</sub>-modified separator is 0.070 and 0.112 mAh cm<sup>−2</sup>, respectively. During the anodic scan (oxidation, i.e., Li dissolution), charges

of 0.042 and 0.085 mAh cm<sup>-2</sup> are passed. Based on these values, comparing the CE of the electrochemical processes (60.0% vs 75.9%) indicates a similar behavior as compared to the constant current measurements where the cells with LiNO<sub>3</sub>-modified separator showed higher capacities in the initial Li electrodisolution step compared to the cells with pristine separator. The higher oxidation current in the CV implies also faster kinetics of the Li electrodeposition/dissolution processes when LiNO<sub>3</sub> is present in the electrolyte solution. This is further confirmed by the values of the exchange current densities ( $i_0$ ) calculated from the Tafel plots obtained from LSV measurements of Li || Li-symmetric cells (Figure 4d). The results indicate that  $i_0$  for Li electrodeposition/dissolution is 0.01 mA cm<sup>-2</sup> for the cell with the unmodified separator and 0.58 mA cm<sup>-2</sup> for the cell containing a LiNO<sub>3</sub> modified separator. The higher value of the  $i_0$  with a LiNO<sub>3</sub>-modified separator strongly implies a faster interfacial charge-transfer process that is in accordance with the observations from the CV measurements (Figure 4c).

Based on the presented results, we assume that the modification of the separator with LiNO<sub>3</sub> maintains a constant concentration of LiNO<sub>3</sub> in the electrolyte, possibly near the saturation level of LiNO<sub>3</sub> in the used electrolyte. To confirm the proposed mechanism of LiNO<sub>3</sub> dissolution into the electrolyte as well as its action as a sacrificial additive, an analytical investigation was carried out, and the results of these investigations are summarized in Figure 5.

Ion chromatography with conductivity detection was used to determine the nitrate concentration in the electrolyte after different numbers of cycles. The electrolyte was recovered from both Cu || Li cells with modified separator and cells with saturated LiNO<sub>3</sub> solution and unmodified separator in order to compare the concentration behavior during cycling. The nitrate concentration of a saturated solution of LiNO<sub>3</sub> dissolved in LP57 was found to be ≈57 mmol L<sup>-1</sup>. Starting from this value, the concentration curve (Figure 5a, black) shows an exponential decrease in nitrate concentration as cycling proceeds. After ten cycles, the concentration of nitrate decreases to ≈35 mmol L<sup>-1</sup> and continues to decrease further to ≈2 mmol L<sup>-1</sup> after 60 cycles. Such behavior highlights the role of a sacrificial additive that LiNO<sub>3</sub> plays in Li metal-based cells. In contrast, the concentration of nitrate in the electrolyte from the cells with LiNO<sub>3</sub>-enriched separators remains nearly constant during cycling. After 60 cycles, the amount of nitrate in the electrolyte was found to be ≈41 mmol L<sup>-1</sup>, compared to ≈50 mmol L<sup>-1</sup> at the beginning of the experiment ( $t = 0$ ). These results show that the LiNO<sub>3</sub> stored in the separator is continuously dissolved into the electrolyte, maintaining a nearly saturated solution of LiNO<sub>3</sub> in LP57. In this way, the beneficial effect of the protective SEI layer on the LMA is longer maintained. Therefore, the LiNO<sub>3</sub>-enriched separator acts as a reservoir, which enables long cycle life, fast kinetics, and homogeneous LSAL deposits due to the steady release of LiNO<sub>3</sub>.

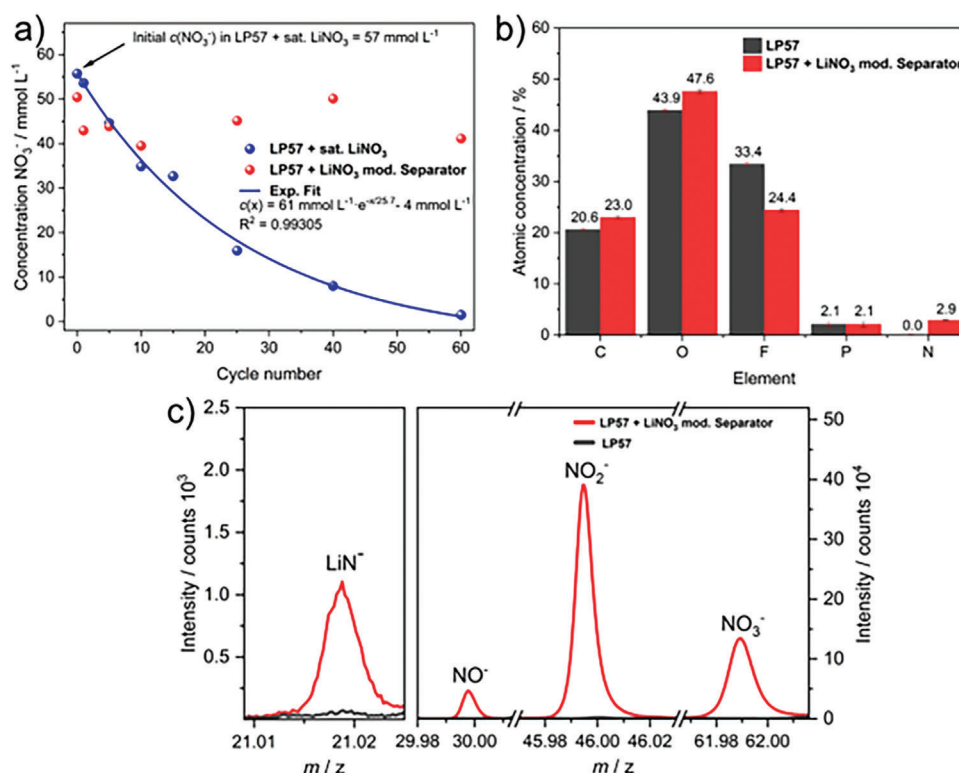


**Figure 5.** a) Comparison between the nitrate concentration after cycling in Cu || Li cells with saturated LiNO<sub>3</sub> in LP57 and LiNO<sub>3</sub> modified separator. b) Relative atomic concentrations of the deposited layer on the copper electrode in Cu || Li cells with LP57 without and with a LiNO<sub>3</sub> modified separator after 20 cycles, determined via EDX measurements. c) Excerpt of ToF-SIMS spectra of the deposition layer on the copper electrode after 20 cycles in Cu || Li cells with LP57 without and with a LiNO<sub>3</sub>-modified separator.



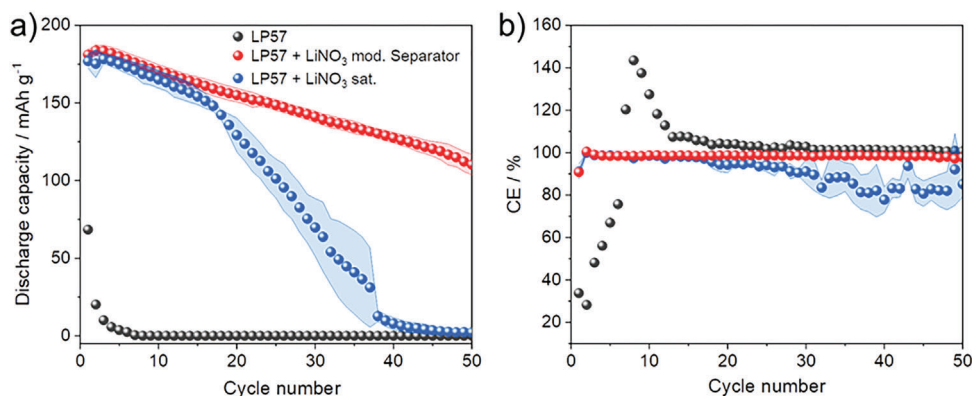


**Figure 6.** Electrochemical cycling results of NCM622 || Cu cells showing a) the evolution of the specific discharge capacities and b) Coulombic efficiencies. The comparison shows cells with only LP57 electrolyte (grey), LiNO<sub>3</sub>-modified separator (red), and LiNO<sub>3</sub>-saturated electrolyte (blue) cycled at a C-rate of 0.2C between 3.0 V ≤ U ≤ 4.3 V at 40 °C.

During cycling, LiNO<sub>3</sub> forms different decomposition products that lead to an increased nitrogen content in the SEI, inducing different chemical properties on the LMA's surface. The elemental composition of the Cu electrode surface after 20 cycles without and with LiNO<sub>3</sub> modification of the separator was investigated by EDX measurements (Figure 5b). Qualitative indication of the main surface components is in accordance with the previous reports.<sup>[40,53]</sup> The results show the presence of oxygen, fluorine, and carbon species at the surface that originate from the electrolyte, with a small portion of phosphorus (2.1% ± 0.5%) from the conductive salt LiPF<sub>6</sub>. Cu || Li cells cycled with a pristine separator have no source of nitrogen while the separator enriched with LiNO<sub>3</sub> leads to a relative nitrogen content of 2.9% ± 0.1%, indicating the formation of nitrogen-containing species on the electrodes' surface (Cu || Li) during cycling.

ToF-SIMS was carried out to investigate the chemical composition of the nitrogen species deposited on the copper electrode after 20 cycles in Cu || Li cells without and with LiNO<sub>3</sub> modification to the separator (Figure 5c). Besides nitrate itself, reduced nitrate species such as NO<sub>2</sub><sup>-</sup>, NO<sup>-</sup>, and LiN<sup>-</sup> are present in the cell with a LiNO<sub>3</sub>-modified separator, which supports the assumption that NO<sub>3</sub><sup>-</sup> is reduced during cycling on the electrode surface. It should be noted that the reduced nitrate species could also be formed by the decomposition of nitrate as a result of the collision with primary ions. The peak area of each nitrate species measured on five different spots at the copper electrode shows that the intensity of the reduced nitrate species of the cells cycled with LiNO<sub>3</sub> modified separator are magnitudes higher compared to the cell without LiNO<sub>3</sub> (Figure S6, Supporting Information).

The effect of LiNO<sub>3</sub> on the passivation of Li metal surfaces has been thoroughly studied in the literature and the surface layer was often described as Li<sub>x</sub>NO<sub>y</sub> species, as first suggested by Aurbach et al.<sup>[55]</sup> It is known that an inorganic-rich SEI contributes to a lower energy barrier for the interfacial/interphasial transport of Li<sup>+</sup>, resulting in lower overpotentials and dense Li deposits. Moreover, the reduced nitrate species Li<sub>3</sub>N shows high Li<sup>+</sup> conductivity (6.6 × 10<sup>-7</sup> mS cm<sup>-1</sup>) which is much higher compared to LiF (10<sup>-10</sup>–10<sup>-11</sup> mS cm<sup>-1</sup>), leading to a decreased interfacial/interphasial resistance during cycling and faster Li<sup>+</sup> transport through the SEI.<sup>[56–58]</sup> In 2015, Guo et al.<sup>[59]</sup> reported the chemical composition of the SEI at LMA in a carbonate-based sys-

tem (1 M LiPF<sub>6</sub> in EC/DMC + VC) with LiNO<sub>3</sub> as an additive. Li<sub>3</sub>N and LiNO<sub>2</sub> were found to be the dominant nitrogen-containing species. LMAs assembled in cell systems with LiNO<sub>3</sub> and ether-based electrolytes lead to the formation of Li<sub>x</sub>N<sub>y</sub>, Li<sub>3</sub>N, LiNO<sub>2</sub>, and LiNO<sub>3</sub> as part of the SEI<sup>[47,51,60]</sup> that are the same species found in this work.

Three different cell types with NCM622 || Cu were cycled to investigate the influence of LiNO<sub>3</sub> on the cycling behavior of ZELMBs, and the results are provided in Figure 6.

In contrast to the Cu || Li cells, the total amount of electrochemically active Li in ZELMBs originates only from the CAM. Therefore, consumption of the electrochemically active Li by irreversible side reactions induces a rapid capacity fading. This can easily be observed for the cells containing only LP57, which lose 98% of their capacity within the first ten cycles (Figure 6a; Figures S7 and S8, Supporting Information). On the other side, the capacity of the cells containing LiNO<sub>3</sub> is fading more slowly, with the lowest slope for cells with LiNO<sub>3</sub>-modified separators. Both LiNO<sub>3</sub>-containing cells initially behave similarly, showing a slight decrease in the discharge capacity due to the loss of small amounts of active lithium. However, the cell with electrolyte-saturated LiNO<sub>3</sub> shows a sharp capacity drop after cycle 18 suggesting that a decrease of the LiNO<sub>3</sub> concentration in the electrolyte occurs during cycling. Since the cells with the LiNO<sub>3</sub> modified separators are able to continuously supply LiNO<sub>3</sub> to the electrolyte, their Li inventory retention is obviously improved. Finally, this leads to a remaining discharge capacity of 110 mAh g<sup>-1</sup> after 50 cycles (62% capacity retention). Regarding the CE of the electrochemical processes, the reference cell shows a poor first-cycle CE of only 37%, while both cells using LiNO<sub>3</sub> show CEs of 91%, 100%, and 99% in the first three cycles (Figure 6b). Overall, the cycling behavior of the three different cells can be compared with and associated with the results from the nitrate concentration determination via ion chromatography. The drop of the nitrate concentration after the 15 cycles is mirrored in the capacity drop of the cells with LiNO<sub>3</sub>-saturated electrolyte.

In summary, the LiNO<sub>3</sub> addition to the separator leads to the presence of a constant concentration of LiNO<sub>3</sub> in the electrolyte, resulting in an improved SEI on the Li deposits with less dead lithium and HSAL formation, which is depicted schematically in Figure 7.

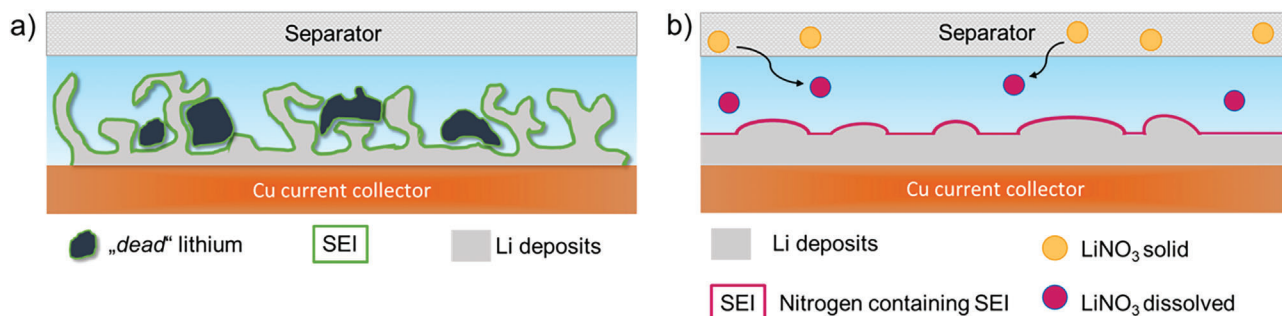


**Figure 7.** Schematic representation during Li electrodeposition/dissolution a) in LP57 conventional carbonate-based electrolyte without  $\text{LiNO}_3$  and b) when  $\text{LiNO}_3$  is added to the separator to maintain a constant concentration in the electrolyte.

The absence of  $\text{LiNO}_3$  in the electrolyte results in the formation of HSAL and dead lithium deposits that accumulate on the Cu substrate upon cycling, leading to the premature failure of the ZELMB (Figure 7a). On the other side, the constant presence of  $\text{LiNO}_3$  supplied to the electrolyte from the separator, maintains a stable SEI on the negative electrodes and thus also a stable capacity retention with improved CE and dense Li deposits (Figure 7b). Nevertheless, although the addition of  $\text{LiNO}_3$  enhances the capacity retention compared to the reference electrolyte, material engineering (e.g., Cu substrate's coatings and morphology) is needed in order to further advance the technological breakthrough of ZELMBs with liquid electrolytes.

### 3. Conclusion

In this work, the enrichment of commercially available separators with  $\text{LiNO}_3$  was investigated in ZELMBs using Cu || Li and NCM622 || Li cell configurations with carbonate-based electrolyte (LP57). The cells with  $\text{LiNO}_3$ -modified separators show superior performance compared to those with unmodified separators. Furthermore, the approach of using  $\text{LiNO}_3$  precipitated in the separator rather than as an electrolyte additive in carbonate-based electrolytes positively affects the cycling stability. In Cu || Li cells,  $\text{LiNO}_3$ -modified separator leads to an extended cycle life with lower overpotentials and increased CE compared to the cells with unmodified separators. Postmortem analysis indicates that the morphology of the lithium deposits is mossy and highly porous in the cells using the unmodified separator, while dense and well-packed lithium deposits are formed for the cells containing the  $\text{LiNO}_3$ -modified separators. The investigations of NCM622 || Cu cells indicate a prolonged cycle life with better capacity retention when  $\text{LiNO}_3$  is added to the separator. With the help of IC measurements, we show that the concentration of  $\text{LiNO}_3$  remains almost constant in the electrolyte when  $\text{LiNO}_3$  is present in the separator rather than in the electrolyte. Based on the results presented here, we can conclude the following key points: a) the presence of  $\text{LiNO}_3$  in the electrolyte is beneficial for the morphology of the Li deposits, resulting in improved CEs, b) the addition of  $\text{LiNO}_3$  in the separator rather than in the carbonate-based electrolyte allows an increase of the duration over which the  $\text{LiNO}_3$  is present in the electrolyte, keeping in mind the sacrificial effect of  $\text{LiNO}_3$  as electrolyte additive, and c) the presence of  $\text{LiNO}_3$  in NMC || Cu cells (i.e., ZELMBs) indicates the importance of electrolyte additives in stabilizing the cycling performance of

ZELMBs with liquid electrolytes. Although this work shows an elegant way to use  $\text{LiNO}_3$  with carbonate electrolytes for ZELMBs, there is still much improvement needed in order to further stabilize the capacity fading mechanism observed in ZELMBs with liquid electrolytes.

### 4. Experimental Section

**Preparation of  $\text{LiNO}_3$ -Modified Separators:** A solution of 207 mg  $\text{LiNO}_3$  (99%, abcr GmbH) dissolved in 1,2-dimethoxyethane (DME, 99%, Sigma-Aldrich), corresponding to a concentration of 0.3 M, was used to prepare the  $\text{LiNO}_3$  modified separators. The separator stack, two inner layers of Freudenberg 2190 (FS 2190, Freudenberg), and two outer layers of Celgard 2500 (Cg 2500, Celgard) with 14 mm in diameter were then wetted with 120  $\mu\text{L}$  of the  $\text{LiNO}_3$  solution. After the solvent was removed under vacuum ( $\approx 10^{-3}$  mbar), the  $\text{LiNO}_3$ -modified separators were further used for the assembly of electrochemical cells. For the assembly of the electrochemical cells, separator stacks were punched into stacks with smaller diameters (13 and 10 mm).

**Electrochemical Measurements:** To carry out the electrochemical investigations, CR 2032-type coin cells and T-cells (SWAGELOK) were assembled using Cu foil (Schlenk metal foils GmbH), Li foil (Honjo Metal, 12 mm diameter, 150  $\mu\text{m}$  thickness, 30.9  $\text{mAh cm}^{-2}$ ) and  $\text{LiNi}_{0.6}\text{Co}_{0.2}\text{Mn}_{0.2}\text{O}_2$  (NCM622, active material loading  $\approx 12.83 \text{ mg cm}^{-2}$ , BASF) electrodes with a diameter of 12 mm. The separator stack (pristine or  $\text{LiNO}_3$  modified) was wetted by 80  $\mu\text{L}$  of a carbonate electrolyte based on 1 M  $\text{LiPF}_6$  in EC/EMC 3:7 (wt:wt) (LP57, BASF). The  $\text{LiNO}_3$ -saturated electrolyte solution was prepared by adding 2 g of  $\text{LiNO}_3$  to 10 mL electrolyte solution and was stirred overnight. After the remaining solid was removed by filtration, the obtained liquid electrolyte (denoted further as LP57 +  $\text{LiNO}_3$  sat.) was further used for the electrochemical experiments. Li electrodeposition and dissolution in Cu ||  $\text{Li}^{[44]}$  cells were carried out using current densities of 0.5 and 1.25  $\text{mA cm}^{-2}$  while for Li || Li cells a current density of 1.0  $\text{mA cm}^{-2}$  was applied. The current density of Cu || Li cells was set to 0.05  $\text{mA cm}^{-2}$  to observe the  $\text{LiNO}_3$  decomposition in constant current experiments. The total amount of transported capacity/step was fixed to 1  $\text{mAh cm}^{-2}$  in all experiments. Galvanostatic cycling of NCM622 || Cu ZELMB cells was performed with a C-rate of 0.2C (where 1C = 180  $\text{mA g}^{-1}$ ) for both charge and discharge steps within a voltage range of 3.0 V  $\leq U \leq$  4.3 V at 40  $^\circ\text{C}$ . All constant current measurements were carried out on a Maccor 4000 battery testing unit (MACCOR) and a climate control chamber (BINDER KB 400).

**Electrochemical Reactions Investigations:** Cyclic voltammetry (CV) of the electrolyte solutions was performed in Cu || Li cells by scanning the voltage range of OCV  $\leq U \leq$  -0.5 V with a scan rate of 10  $\text{mV s}^{-1}$ . Linear sweep voltammetry of various electrolytes was carried out in Li || Li-symmetric cells by using a sweep rate of 2  $\text{mV s}^{-1}$  from the initial voltage



of  $-0.2 \text{ V} \leq U \leq 0.2 \text{ V}$ . The exchange current density ( $i_0$ ) was determined from the resulting Tafel plots. Cyclic voltammetry using a 3-electrode setup was performed in Cu || Li with Li as reference electrode with a scan rate of  $1 \text{ mV s}^{-1}$  within a potential range of  $0.0 \text{ V} \leq E \leq 2.5 \text{ V}$  versus  $\text{Li}|\text{Li}^+$ . Prior to all measurements, a rest step was performed for 3 h. All measurements were performed at  $20^\circ\text{C}$  using a VSP Potentiostat (BioLogic Inc).

**Morphological Investigation:** Scanning electron microscopy (SEM) images and cryo-focused-ion beam (FIB) of the Li deposits were obtained by a Zeiss Crossbeam 550 electron microscope (cryo-FIB-SEM, Carl Zeiss Microscopy GmbH). Images were taken at 3 kV accelerating voltage and with an aperture size of  $30 \mu\text{m}$  using an in-lens detector with a working distance of  $\approx 5 \text{ mm}$ . The acquisition time was optimized so that the electron beam did not induce any surface changes during exposure at high magnifications ( $>2500\times$ ). The cryo-FIB cross-sections were performed with an accelerating voltage of 30 kV and a current ranging from 7 to 30 nA at a temperature of  $-160^\circ\text{C}$  to maintain the morphology of the samples mounted on a specialized sample holder setup (Kammrath & Weiss GmbH). To prevent air exposure, all Li-metal samples were transferred using a vacuum-sealed sample holder. The elemental composition of the electrode surface was investigated by energy-dispersive X-ray spectroscopy (EDX) with an Ultim Extrem detector (Oxford Instruments) and evaluated using the AZtech software (Oxford Instruments). The spectra were recorded with an acceleration voltage of 3.0 kV.

**$\text{LiNO}_3$  Concentration Determination:** Ion chromatography (IC) was performed on an 850 Professional IC (Metrohm) with conductivity detection (CD). A Metrosep A Supp 7 ( $250 \times 4.0 \text{ mm}$ ,  $5 \mu\text{m}$ , Metrohm) separation column coupled with a Metrosep A Supp 4/5 guard column was used for isocratic anion separation at  $65^\circ\text{C}$  and a flow rate of  $0.7 \text{ mL min}^{-1}$  was applied. The eluent consisted of 58:42 (vol. ratio)  $3.6 \text{ mM Na}_2\text{CO}_3$  :  $3.4 \text{ mM NaHCO}_3$  aqueous solution and acetonitrile with a run time of 30 min. Electrolytes were diluted 1:100 prior to investigation and the injection volume was  $65 \mu\text{L}$ . The Metrohm suppressor module was sequentially generated with  $0.1 \text{ mol L}^{-1}$  sulfuric acid (95–97%, EMSURE, Merck KGaA) and flushed with MilliQ water in a 30 min interval. The employed method is based on Kraft et al.<sup>[45]</sup> and further parameters were applied according to Henschel et al.<sup>[46]</sup>

**LMA Surface Composition Investigation:** Time-of-flight secondary ion mass spectrometry (ToF-SIMS) measurements were performed on a TOF-SIMS 5 instrument (IonToF GmbH) equipped with a 30 keV bismuth (Bi) primary ion source and 500 eV Cs sputter ion source. For analysis, the primary ion source was tuned in the spectrometry mode (bunched mode) for high mass resolution. The analysis was performed in a  $100 \times 100 \mu\text{m}^2$  field of view, rastered with  $128 \times 128$  pixels.  $\text{Bi}^{3+}$  ions were used as primary ions at an ion current of 1.9 pA. During the measurement, the surface was sputtered with  $\text{Cs}^+$  sputter ions at an ion current of 40 nA. The mass analyzer was operated in the negative ion mode. For each sample, a set of five measurements at different positions was performed. Measurement was stopped after 60 scans. Data evaluation was carried out in the Surface-Lab 7.2 software (IonToF GmbH).

## Supporting Information

Supporting Information is available from the Wiley Online Library or from the author.

## Acknowledgements

The authors would like to acknowledge the financial support from the German Federal Ministry of Education and Research (BMBF) within the projects MEET-HiEnD III (03XP0258A) and ProLiFest (03XP0253A).

Silvan Stuckenberg and Verena Küpers acknowledge the financial support from the German Research Foundation (DFG) under the project number 509322222.

Open access funding enabled and organized by Projekt DEAL.

## Conflict of Interest

The authors declare no conflict of interest.

## Data Availability Statement

The data that support the findings of this study are available from the corresponding author upon reasonable request.

## Keywords

extended cycle life, lithium deposits, lithium–metal batteries, lithium nitrate, zero-excess lithium metal batteries

Received: June 21, 2023  
Revised: September 4, 2023  
Published online: October 5, 2023

- [1] M. Winter, B. Barnett, K. Xu, *Chem. Rev.* **2018**, *118*, 11433.
- [2] J. M. Tarascon, M. Armand, *Nature* **2001**, *414*, 359.
- [3] Y. Nishi, *Chem. Rev.* **2001**, *1*, 406.
- [4] Z. Li, J. Huang, B. Yann Liaw, V. Metzler, J. Zhang, *J. Power Sources* **2014**, *254*, 168.
- [5] J. Liu, Z. Bao, Y. Cui, E. J. Dufek, J. B. Goodenough, P. Khalifah, Q. Li, B. Y. Liaw, P. Liu, A. Manthiram, Y. S. Meng, V. R. Subramanian, M. F. Toney, V. V. Viswanathan, M. S. Whittingham, J. Xiao, W. Xu, J. Yang, X.-Q. Yang, J.-G. Zhang, *Nat. Energy* **2019**, *4*, 180.
- [6] D. Lin, Y. Liu, Y. Cui, *Nat. Nanotechnol.* **2017**, *12*, 194.
- [7] J. R. Nair, L. Imholt, G. Brunklaus, M. Winter, *Electrochem. Soc. Interface* **2019**, *28*, 55.
- [8] A. J. Louli, M. Genovese, R. Weber, S. G. Hames, E. R. Logan, J. R. Dahn, *J. Electrochem. Soc.* **2019**, *166*, A1291.
- [9] R. Schmuck, R. Wagner, G. Höpkel, T. Placke, M. Winter, *Nat. Energy* **2018**, *3*, 267.
- [10] B. Wu, Y. Yang, D. Liu, C. Niu, M. Gross, L. Seymour, H. Lee, P. M. L. Le, T. D. Vo, Z. D. Deng, E. J. Dufek, M. S. Whittingham, J. Liu, J. Xiao, *J. Electrochem. Soc.* **2019**, *166*, A4141.
- [11] C. Niu, D. Liu, J. A. Lochala, C. S. Anderson, X. Cao, M. E. Gross, W. Xu, J.-G. Zhang, M. S. Whittingham, J. Xiao, J. Liu, *Nat. Energy* **2021**, *6*, 723.
- [12] H. Chen, Y. Yang, D. T. Boyle, Y. K. Jeong, R. Xu, L. S. de Vasconcelos, Z. Huang, H. Wang, H. Wang, W. Huang, H. Li, J. Wang, H. Gu, R. Matsumoto, K. Motohashi, Y. Nakayama, K. Zhao, Y. Cui, *Nat. Energy* **2021**, *6*, 790.
- [13] K. Schönherr, B. Schumm, F. Hippauf, R. Lissy, H. Althues, C. Leyens, S. Kaskel, *Chem. Eng. J. Adv.* **2022**, *9*, 100218.
- [14] F. Duffner, N. Kronmeyer, J. Tübke, J. Leker, M. Winter, R. Schmuck, *Nat. Energy* **2021**, *6*, 123.
- [15] C.-J. Huang, B. Thirumalraj, H.-C. Tao, K. N. Shitaw, H. Sutiono, T. T. Hagos, T. T. Beyene, L.-M. Kuo, C.-C. Wang, S.-H. Wu, W.-N. Su, B. J. Hwang, *Nat. Commun.* **2021**, *12*, 1452.
- [16] J. Qian, B. D. Adams, J. Zheng, W. Xu, W. A. Henderson, J. Wang, M. E. Bowden, S. Xu, J. Hu, J.-G. Zhang, *Adv. Funct. Mater.* **2016**, *26*, 7094.
- [17] H. Ye, Y. Zhang, Y.-X. Yin, F.-F. Cao, Y.-G. Guo, *ACS Cent. Sci.* **2020**, *6*, 661.
- [18] A. Rosenman, R. Elazari, G. Salitra, E. Markevich, D. Aurbach, A. Garsuch, *J. Electrochem. Soc.* **2015**, *162*, A470.
- [19] D.-J. Yoo, A. Elabd, S. Choi, Y. Cho, J. Kim, S. J. Lee, S. H. Choi, T.-w. Kwon, K. Char, K. J. Kim, A. Coskun, J. W. Choi, *Adv. Mater.* **2019**, *31*, 1901645.

- [20] X. Wang, W. Zeng, L. Hong, W. Xu, H. Yang, F. Wang, H. Duan, M. Tang, H. Jiang, *Nat. Energy* **2018**, 3, 227.
- [21] X. Gao, X. Yang, K. Adair, X. Li, J. Liang, Q. Sun, Y. Zhao, R. Li, T.-K. Sham, X. Sun, *Adv. Energy Mater.* **2020**, 10, 1903753.
- [22] J. Chen, J. Zhao, L. Lei, P. Li, J. Chen, Y. Zhang, Y. Wang, Y. Ma, D. Wang, *Nano Lett.* **2020**, 20, 3403.
- [23] R. Zhu, C. Zhu, N. Sheng, Z. Rao, Y. Aoki, H. Habazaki, *Chem. Eng. J.* **2020**, 388, 124256.
- [24] A. A. Assegie, C.-C. Chung, M.-C. Tsai, W.-N. Su, C.-W. Chen, B.-J. Hwang, *Nanoscale* **2019**, 11, 2710.
- [25] S. S. Zhang, X. Fan, C. Wang, *Electrochim. Acta* **2017**, 258, 1201.
- [26] C. Jin, O. Sheng, J. Luo, H. Yuan, C. Fang, W. Zhang, H. Huang, Y. Gan, Y. Xia, C. Liang, J. Zhang, X. Tao, *Nano Energy* **2017**, 37, 177.
- [27] R. Weber, M. Genovese, A. J. Louli, S. Hames, C. Martin, I. G. Hill, J. R. Dahn, *Nat. Energy* **2019**, 4, 683.
- [28] A. J. Louli, A. Eldesoky, R. Weber, M. Genovese, M. Coon, J. deGooyer, Z. Deng, R. T. White, J. Lee, T. Rodgers, R. Petibon, S. Hy, S. J. H. Cheng, J. R. Dahn, *Nat. Energy* **2020**, 5, 693.
- [29] H. Choi, Y. Bae, S.-M. Lee, Y.-C. Ha, H.-C. Shin, B. G. Kim, *J. Electrochem. Sci. Technol.* **2022**, 13, 78.
- [30] T. T. Beyene, H. K. Bezabh, M. A. Weret, T. M. Hagos, C.-J. Huang, C.-H. Wang, W.-N. Su, H. Dai, B.-J. Hwang, *J. Electrochem. Soc.* **2019**, 166, A1501.
- [31] A. Eldesoky, A. J. Louli, A. Benson, J. R. Dahn, *J. Electrochem. Soc.* **2021**, 168, 120508.
- [32] R. M. Kasse, N. R. Geise, J. S. Ko, J. Nelson Weker, H.-G. Steinrück, M. F. Toney, *J. Mater. Chem. A* **2020**, 8, 16960.
- [33] L. Su, H. Charalambous, Z. Cui, A. Manthiram, *Energy Environ. Sci.* **2022**, 15, 843.
- [34] W.-T. Xu, H.-J. Peng, J.-Q. Huang, C.-Z. Zhao, X.-B. Cheng, Q. Zhang, *ChemSusChem* **2015**, 8, 2892.
- [35] Q. Pang, X. Liang, C. Y. Kwok, J. Kulisch, L. F. Nazar, *Adv. Energy Mater.* **2017**, 7, 1601630.
- [36] D. Moy, A. Manivannan, S. R. Narayanan, *J. Electrochem. Soc.* **2015**, 162, A1.
- [37] L. Cheng, L. A. Curtiss, K. R. Zavadil, A. A. Gewirth, Y. Shao, K. G. Gallagher, *ACS Energy Lett.* **2016**, 1, 503.
- [38] B. D. Adams, E. V. Carino, J. G. Connell, K. S. Han, R. Cao, J. Chen, J. Zheng, Q. Li, K. T. Mueller, W. A. Henderson, J.-G. Zhang, *Nano Energy* **2017**, 40, 607.
- [39] D. W. Kang, J. Moon, H.-Y. Choi, H.-C. Shin, B. G. Kim, *J. Power Sources* **2021**, 490, 229504.
- [40] Q. Shi, Y. Zhong, M. Wu, H. Wang, H. Wang, *Proc. Natl. Acad. Sci. USA* **2018**, 115, 5676.
- [41] B. A. Jote, K. N. Shitaw, M. A. Weret, S.-C. Yang, C.-J. Huang, C.-H. Wang, Y.-T. Weng, S.-H. Wu, W.-N. Su, B. J. Hwang, *J. Power Sources* **2022**, 532, 231303.
- [42] C.-J. Huang, Y.-C. Hsu, K. N. Shitaw, Y.-J. Siao, S.-H. Wu, C.-H. Wang, W.-N. Su, B. J. Hwang, *ACS Appl. Mater. Interfaces* **2022**, 14, 26724.
- [43] D. Liu, X. Xiong, Q. Liang, X. Wu, H. Fu, *Chem. Commun.* **2021**, 57, 9232.
- [44] R. Nölle, K. Beltrop, F. Holtstiege, J. Kasnatscheew, T. Placke, M. Winter, *Mater. Today* **2020**, 32, 131.
- [45] V. Kraft, M. Grütze, W. Weber, M. Winter, S. Nowak, *J. Chromatogr. A* **2014**, 1354, 92.
- [46] J. Henschel, F. Horsthemke, Y. P. Stenzel, M. Evertz, S. Girod, C. Lürenbaum, K. Kösters, S. Wiemers-Meyer, M. Winter, S. Nowak, *J. Power Sources* **2020**, 447, 227370.
- [47] S. Xiong, K. Xie, Y. Diao, X. Hong, *J. Power Sources* **2014**, 246, 840.
- [48] M. Barghamadi, A. S. Best, A. F. Hollenkamp, P. Mahon, M. Musameh, T. Rütger, *Electrochim. Acta* **2016**, 222, 257.
- [49] A. Jozwiuk, B. Berkes, T. Weiß, H. Sommer, J. Janek, T. Brezesinski, *Energy Environ. Sci.* **2016**, 9, 2603.
- [50] V. Giordani, J. Uddin, V. S. Bryantsev, G. V. Chase, D. Addison, *J. Electrochem. Soc.* **2016**, 163, A2673.
- [51] S. Xiong, K. Xie, Y. Diao, X. Hong, *Electrochim. Acta* **2012**, 83, 78.
- [52] V. Küpers, M. Kolek, P. Bieker, M. Winter, G. Brunklaus, *Phys. Chem. Chem. Phys.* **2019**, 21, 26084.
- [53] S. S. Zhang, *Electrochim. Acta* **2012**, 70, 344.
- [54] C. Day, K. Greig, A. Massey, J. Peake, D. Crossley, R. A. W. Dryfe, *ChemSusChem* **2020**, 13, 1504.
- [55] D. Aurbach, *J. Electrochem. Soc.* **1989**, 136, 906.
- [56] K. Park, J. B. Goodenough, *Adv. Energy Mater.* **2017**, 7, 1700732.
- [57] H. Yildirim, A. Kinaci, M. K. Y. Chan, J. P. Greeley, *ACS Appl. Mater. Interfaces* **2015**, 7, 18985.
- [58] B. A. Boukamp, R. A. Huggins, *Mater. Res. Bull.* **1978**, 13, 23.
- [59] J. Guo, Z. Wen, M. Wu, J. Jin, Y. Liu, *Electrochem. Commun.* **2015**, 51, 59.
- [60] M. Barghamadi, A. S. Best, A. I. Bhatt, A. F. Hollenkamp, P. J. Mahon, M. Musameh, T. Rütger, *J. Power Sources* **2015**, 295, 212.